Publication I

Reprinted from Sensors and Actuators A, 125 (2006), p. 281-287, © 2005, with permission from Elsevier

Moisture sensor at glass/polymer interface for monitoring of photovoltaic module encapsulants

T.Carlsson, J.Halme, P.Lund, P.Konttinen

Available online at www.sciencedirect.com
SCIENCE DIRECT
Sensors and Actuators A 125 (2006) 281–287
SENSORS AND ACTUATORS A PHYSICAL
www.elsevier.com/locate/sna

Moisture sensor at glass/polymer interface for monitoring of photovoltaic module encapsulants

Thomas Carlsson *, Janne Halme, Peter Lund, Petri Konttinen

Helsinki University of Technology, Advanced Energy Systems, Rakentajanaukio 2 C, P.O. Box 2200, FIN-02015 HUT, Finland

Received 14 April 2005; received in revised form 6 July 2005; accepted 24 July 2005
Available online 26 September 2005

Abstract

A sensor developed for measurement of water concentration inside glass/polymer encapsulation structures with a particular application area in accelerated aging of photovoltaic module encapsulants is described. An approximately 5 μm thick porous TiO_2 film applied to a glass substrate with a conductive coating acts as the moisture-sensitive component. The response is calibrated with weather chamber experiments for sensors open to the environment and with diffusion experiments for sensors laminated under an encapsulant. For the interpretation of diffusion experiment results, a transport model describing the diffusion of water across the polymer/TiO_2 interface is developed. The logarithm of AC resistance shows a linear dependence on water concentration in both open and encapsulated calibration. The first measurable response from an encapsulated 3.5 mm × 8 mm size sensor is obtained when approximately 10 μg of water has entered the film. Implications of the calibration results for sensor usage in accelerated aging tests are discussed.

Keywords: Moisture sensor; Titanium dioxide; Encapsulation; Photovoltaics; Thin-film

1. Introduction

Photovoltaic (PV) energy is a rapidly growing source of renewable electricity with positive expectations for the future. The competitiveness of PV electricity depends on the efficiency, cost and lifetime of PV modules. All three factors are interdependent. The lifetime-cost trade-off manifests itself in the encapsulation of the PV module, which is normally done with an elastomeric polymer encapsulant. Ethylene vinyl acetate (EVA) is the most widely used encapsulant today. It combines good protection properties with low cost, but its qualities may degrade during long-term usage due to stress factors such as UV-light and high temperatures [1]. Encapsulant degradation usually has an immediate effect on module performance especially if moisture begins to penetrate through the polymer to the active cell materials. The interdependence between moisture penetration and other degradation mechanisms such as photothermal, photooxidative and deacetylation reactions [1–3] and loss of adhesion [4] is an important field of study. This is the case especially in thin-film PV applications where the active solar cell material (∼1–10 μm in thickness) is deposited on a glass substrate and covered with the encapsulant as shown in Fig. 1, making them inherently vulnerable to moisture penetration at the glass/encapsulant interface [5]. The measurement of moisture concentration inside encapsulated test samples which mimic photovoltaic modules would be a valuable complement to accelerated aging tests for thin-film PV modules, but the utility of previously reported methods [6,7] involving commercially available humidity sensors or similar structures is limited by the large size of the sensors. In this paper the development and calibration of a sensor of micrometer thickness deposited by hand on a glass substrate is described. This sensor can be used for measuring moisture concentration at the glass/encapsulant interface and it has been developed specifically for the purpose of performing accelerated aging tests on encapsulant materials for thin-film PV modules. The moisture-sensitive part of the sensor is nanoporous TiO_2, which has also been used in atmospheric humidity sensors [8–10]. The obtained calibration curves can be used for characterization of the water diffusion process at the glass/encapsulant interface, facilitating estimation of the moisture-limited lifetime of thin-film PV modules.

Abbreviations: CPE, constant phase element; EVA, ethylene vinyl acetate; PV, photovoltaic

* Corresponding author. Tel.: +358 9 4513212; fax: +358 9 4513195.
E-mail address: thomas.carlsson@hut.fi (T. Carlsson).

0924-4247/$ – see front matter © 2005 Elsevier B.V. All rights reserved.
doi:10.1016/j.sna.2005.07.022

Nomenclature

A	constant in $c(r)$ equation for encapsulated sensor (g/mm^3)
B	constant in $c(r)$ equation for encapsulated sensor (g/mm^3)
c	water mass concentration in sensor (g/mm^3)
c_F	value of c when r_F is measured (g/mm^3)
c_{sat}	saturation water mass concentration in sensor (g/mm^3)
c_{TiO_2}	mass concentration of TiO_2 in sensor (g/mm^3)
C	water mass concentration in EVA (g/mm^3)
C_{sat}	saturation water mass concentration in EVA (g/mm^3)
D	diffusion coefficient (mm^2/s)
f	frequency in impedance measurement (Hz)
f_0	limiting frequency for blocking impedance (Hz)
J	water flux (g/mm^2 s)
J_0	water flux through sensor/EVA interface (g/mm^2 s)
L	thickness of EVA film (mm)
p	pressure (bar)
p_0	reference pressure in Clausius–Clapeyron equation (bar)
P	porosity
r	scaled logarithm of sensor resistance
r_F	first measured value of r in encapsulated calibration
R	sensor AC resistance (Ω)
R_G	universal gas constant (J/mol K)
R_0	sensor AC resistance extrapolated to RH = 0 (Ω)
RH	relative humidity
s	thickness off sensor (μm)
t	time (h)
t_1	time at which water transfer rate becomes constant (h)
t_2	time at which water transfer rate begins to decrease (h)
T	temperature (°C)
T_a	ambient temperature (°C)
T_0	reference temperature in Clausius–Clapeyron equation (K)
x	EVA thickness coordinate (mm)
Z_I	imaginary component of impedance (Ω)
Z_R	real component of impedance (Ω)
Δh	isosteric heat of adsorption (J/mol)
ρ	density of water (g/mm^3)

2. Experimental

2.1. Sensor preparation and geometry

Sensors were prepared on 1.1 mm thick glass sheets coated with a 150 nm thick indium-tin-oxide layer having 12 Ω/sq sheet resistance. A pattern of conducting electrodes was created on the glass using photolithography with 10 min etching in a solution of 32 vol% HCl and 8.5 vol% HNO_3. The glass was then dipped in a 10 mass% Na_2CO_3 water solution to neutralize the acid on the glass surface. After removal of the photoresist and cleaning, transparent nanocrystalline TiO_2 HT-L paste (anatase, average particle size 9 nm, porosity 50%) made by Solaronix was applied with a glass rod over the electrode area defined with adhesive tape, and the sensor was heated at 170 °C for 1 h to remove solvents from the paste, increase film adhesion to the substrate and improve contact between the TiO_2 nanoparticles. Several different electrode geometries were studied, and the fork geometry shown in Fig. 2 was chosen as the best one in the optimization between small size and low resistance. Fig. 2 shows only 7 fingers on each side for clarity, but the real sensor contained 14 fingers on each side. The width of the fingers and the separation between them was 150 μm. The thicknesses of the prepared TiO_2 films, measured with a Heidenhain MT1201 linear transducer, were in the range 5 ± 3 μm, which is of the same magnitude as the thickness of a thin-film solar cell. Thickness variations reflect the difficulty of repeatable sensor production by a manual method. Film transparency remained good throughout the preparation and lamination process.

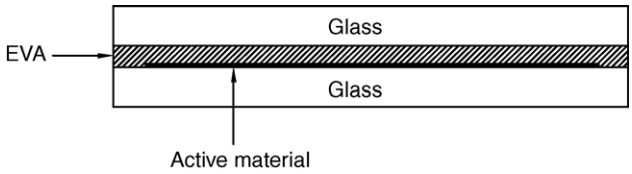

Fig. 1. An encapsulated thin-film PV module. The location of the active material at the glass/EVA interface makes it vulnerable to interfacial moisture penetration.

2.2. Sensor lamination

A layer of 0.5 mm thick EVA (VistaSolar 486.00) with a measured vinyl acetate content of 33 mass% was laminated on top of the sensors in vacuum in a Panamac L A3-A Automatic PV

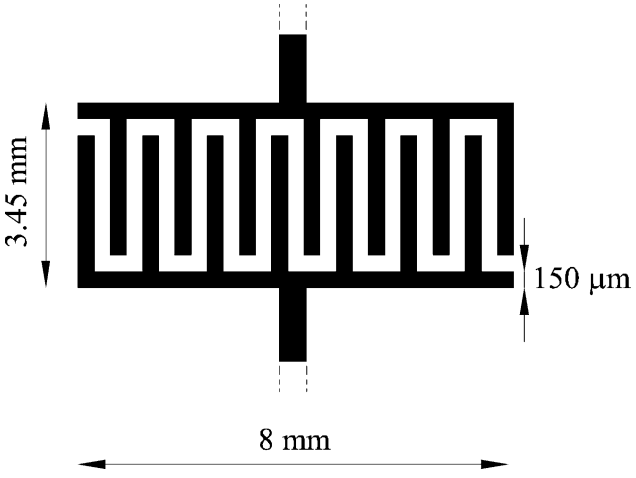

Fig. 2. Geometry of the electrode structure below the TiO_2 film. For clarity, the number of fork fingers has been reduced by half and the smallest dimensions have been enlarged. The width of the fingers and the distance between them is 150 μm.

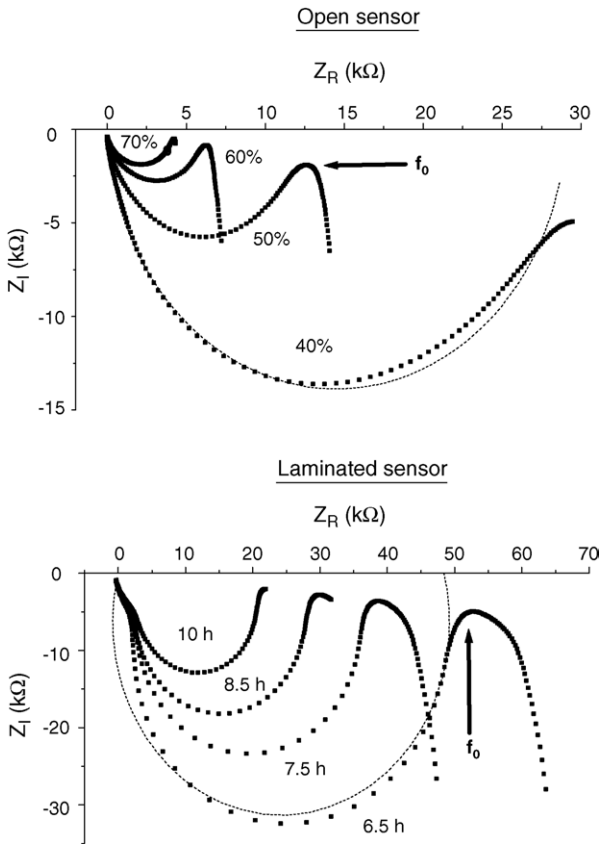

Fig. 3. Nyquist plots of the response of an open sensor as a function of RH at 25 °C, and the response of the same sensor when laminated under EVA as a function of elapsed time since the beginning of a water diffusion experiment. Dashed lines show examples of *R*-CPE equivalent circuit curves fitted to the semicircle data. Two examples of points corresponding to the limiting frequency f_0 are indicated.

Module Laminator. The maximum temperature during lamination was 160 °C.

2.3. Measurement principle

The AC resistance of the sensor is highly sensitive to the water content in the TiO_2 film [11]. To obtain readings from the sensor, its impedance spectrum was measured with a Zahner IM6 Electrochemical Workstation in the 100 Hz to 1 MHz frequency range at zero DC polarization using 500 mV voltage amplitude. As an example, Fig. 3 shows Nyquist plots of measured impedance spectra obtained from a sensor when open to the surroundings at 25 °C in different relative humidity conditions and from the same sensor when laminated under EVA and gradually filled with water which diffused through the EVA at ambient temperature ($T_a = 20 \pm 3$ °C throughout this paper). In both experiments the impedance spectra of the sensor show capacitive (blocking) impedance below a limiting frequency f_0. f_0 increases with water content in the sensor and is in the range 0.5–3 kHz in Fig. 3. The $f < f_0$ parts of the spectra are not shown for all curves since the measurement was sometimes stopped manually when f_0 was reached. At frequencies above f_0, the spectra have a semicircle shape. However, two qualitative differences between the open sensor curves and laminated sensor curves can be distinguished: Firstly, the semicircles of the open sensor curves are depressed whereas the semicircles of the laminated sensor curves are elevated. Secondly, the laminated sensor curves have an approximately linear part at frequencies above 100 kHz. Physical explanations for the capacitive behaviour of the sensor at low frequencies, the depression and elevation of the semicircles and the linear response of the laminated sensors at high frequencies were not sought in this work.

The impedance behaviour of the sensor in both experiments was modeled with an equivalent circuit consisting of sensor resistance (*R*) in parallel with a constant phase element (CPE). Series resistance was negligible compared to parallel resistance and was excluded from the equivalent circuit. Sensor resistance was calculated by fitting the equivalent circuit to the part of the measured curve which displayed semicircle behaviour. The obtained sensor resistance is equivalent to the distance between the real axis intercepts of the semicircle in the Nyquist plot, and it was used as an indicator of the water content of the sensor in this study. Examples of fitted curves used in the determination of *R* are shown with dashed lines in Fig. 3.

3. Sensor calibration

To quantify the dependence of sensor resistance on water content in the sensor, calibration experiments were carried out. These consisted of an atmospheric calibration conducted on open sensors in the weather chamber and an encapsulated calibration where water diffused through the laminated encapsulant and gradually filled the sensor. The latter gives the calibration curve of greatest interest in this application, but the greater flexibility of atmospheric calibration makes it a useful tool for studying the temperature dependence of sensor response.

3.1. Atmospheric calibration

Sensor response was first quantified for sensors open to the surroundings. The response was measured in different temperature (*T*) and relative humidity (RH) conditions in an Arctest ARC-400 weather chamber. Sensor preparation could not be repeated in precisely the same way since it was done manually, and as a consequence a variation in *R* as large as 50% was frequently observed between different sensors. $\lg(R)$ was linearly proportional to relative humidity, and a scaled resistance variable *r* was therefore defined as

$$r = \frac{\lg(R)}{\lg(R_0)}, \quad (1)$$

where $\lg(R_0)$ is the value obtained by extrapolating the $\lg(R)$ versus RH curve to a relative humidity of 0%. The variable *r* was equal between different sensors within an accuracy of 2%. Fig. 4 shows the measured $\lg R$ versus RH and *r* versus RH curves at different temperatures, calculated as an average over six sensors. It is seen that R_0 is higher at 25 °C than at the other temperatures, but the scaled parameter *r* has the same RH dependence at all temperatures. The water mass concentration in the sensor, *c*, in different RH conditions needed to be determined to correlate the

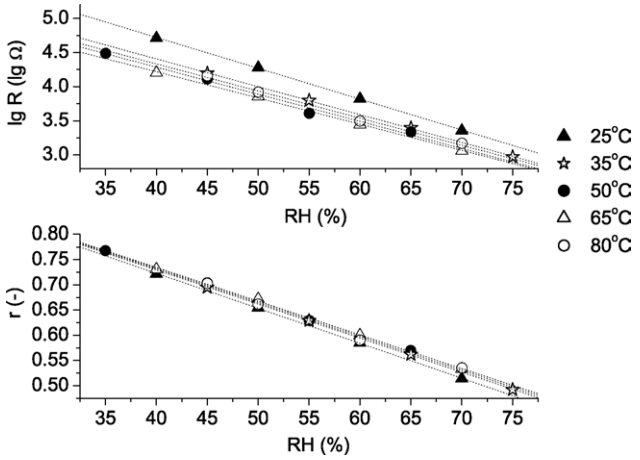

Fig. 4. Results of atmospheric calibration, average curves calculated from six sensors. The r(RH) curves are independent of temperature.

measured r(RH,T) curves in Fig. 4 with the function $r(c,T)$. For this purpose, thermogravimetric measurements were conducted with a Mettler TG50 furnace equipped with an M3 balance. TiO_2 powder was prepared by scraping a film off the glass with a scalpel, and the weight loss of the powder during heating to 162 °C and cooling back to ambient temperature in dry air was measured. The weight loss of the TiO_2 powder corresponds to the loss of adsorbed water. This experiment was repeated in several RH conditions. Fig. 5 shows the relative weight of water in a TiO_2 film, c/c_{TiO_2}, measured at ambient temperature in different relative humidity conditions. At relative humidities above 25%, which is the primary range of interest in this study, c/c_{TiO_2} shows a linear dependence on RH. By taking into account the mass concentration of the TiO_2 film $c_{TiO_2} = (1.1 \pm 0.2)\,\mathrm{mg/mm^3}$, the slope in Fig. 4 ($r = 1 - (0.67 \pm 0.01)$RH) and the linear relation in Fig. 5 ($c/c_{TiO_2} = (0.112 \pm 0.006)$RH), the atmospheric calibration curve in ambient conditions was determined to be

$$r(c) = 1 - (5.4 \pm 1.7)c\,\mathrm{mm^3/mg}. \quad (2)$$

This curve was verified in the RH range 25–75%, corresponding to c values in the range 3–9 mg/mm^3.

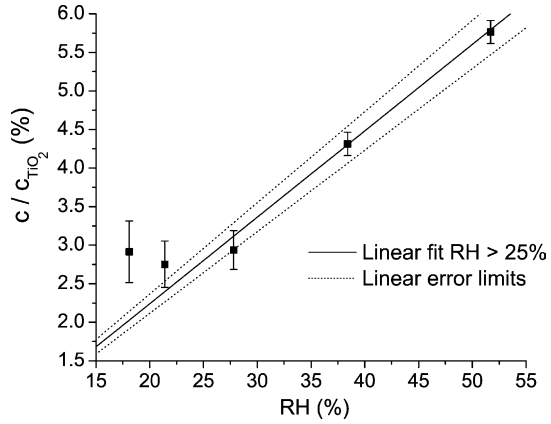

Fig. 5. Fraction of water mass in the sensor vs. relative humidity in the air. Measurements were conducted at ambient temperature. At RH >25%, the relationship is linear.

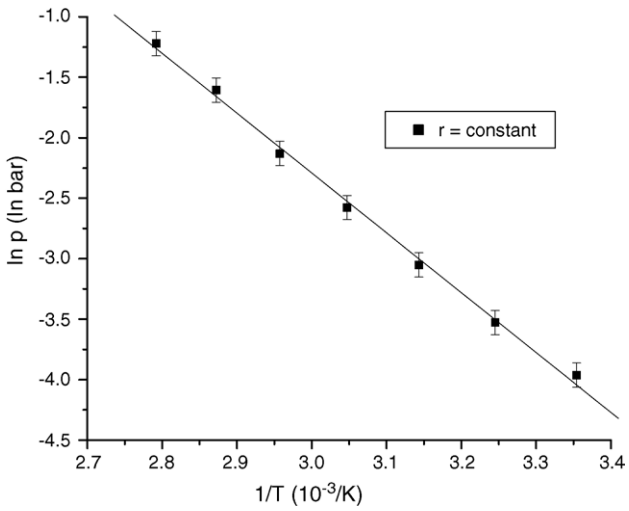

Fig. 6. Plot of the logarithm of water vapor pressure vs. inverse of temperature, collected at a constant value of sensor resistance. Since the points form a straight line with a reasonable value for Δh, the adsorption process obeys Eq. (3) and the condition r = constant corresponds to c = constant.

The applicability of this equation at other temperatures was verified as follows. The Clausius–Clapeyron equation which can be used to describe adsorption of water vapor in porous materials is [12]

$$\ln\left(\frac{p}{p_0}\right) = \frac{\Delta h}{R_G}\left(\frac{1}{T} - \frac{1}{T_0}\right), \quad (3)$$

where p is the water vapor pressure; p_0 and T_0, the reference water vapor pressure and temperature; Δh, the isosteric heat of adsorption and R_G is the universal gas constant. The equation is derived from the assumption that the amount of adsorbed water, in this case c, is the same in all (p,T) conditions. In this experiment, (p,T) values at which the r value of a sensor in the weather chamber remained constant were recorded. Fig. 6 shows these data points, and a linear fit yields a value of −41.1 kJ/mol for Δh. This value is within the range of Δh values measured in [13] for water adsorption in anatase TiO_2 at different degrees of surface coverage, and it can be concluded that the condition r = constant is equivalent to the condition c = constant. The fact that r(RH) in Fig. 4 is independent of temperature therefore indicates that the function c(RH) also is independent of temperature and Eq. (2) is valid at all temperatures of interest in this study.

3.2. Encapsulated calibration

The definition given in Eq. (1) for r was employed also for encapsulated sensors by determining R_0 at 25 °C in the weather chamber before lamination. The moisture response of the sensor when laminated under EVA was characterized with a water diffusion experiment as illustrated in Fig. 7. Distilled water was poured on top of the EVA layer and sensor response as a function of time, $r(t)$, was measured while the water diffused through the EVA into the sensor. The thickness of the EVA layer above each sensor was measured separately and was in the range

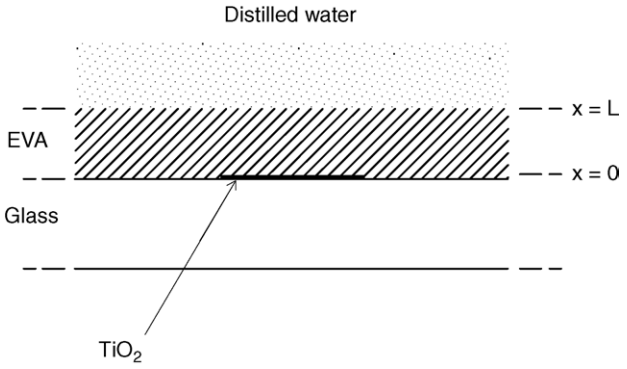

Fig. 7. Setup of the diffusion experiment for encapsulated calibration and definition of the x coordinate. Sensor response was measured as a function of time as water diffused towards the glass/EVA interface. $x = 0$ at the interface between the EVA and the TiO_2.

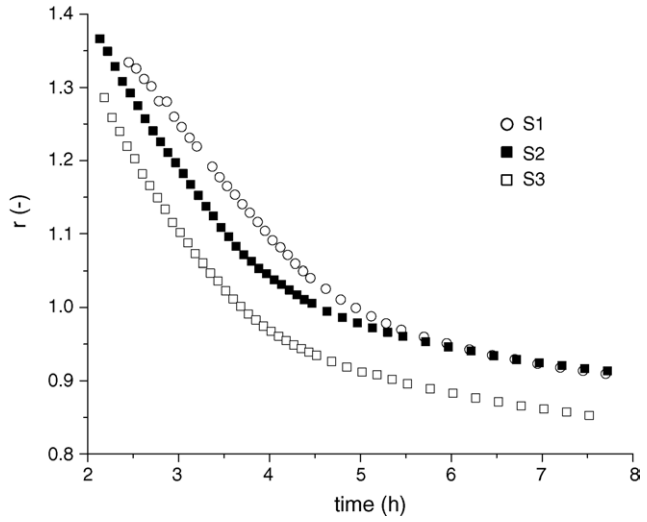

Fig. 8. Response of three encapsulated sensors as a function of time since the beginning of the diffusion experiment.

0.45–0.55 mm. Water diffusion through the EVA is described by the one-dimensional diffusion equation

$$\frac{\partial C}{\partial t} = -\frac{\partial J}{\partial x} = D\frac{\partial^2 C}{\partial x^2}, \tag{4}$$

where C is the water mass concentration in the EVA; J, the water flux; D, the diffusion coefficient of water in EVA and the coordinate x is defined as in Fig. 7 with its zero point at the EVA/TiO_2 interface. The initial condition $C(x,0) = 0$ was assumed throughout the EVA. During the experiment, c is determined by the flux J_0 through the interface at $x = 0$ and can be written as

$$c(t) = \frac{\int_0^t J_0\,\mathrm{d}t}{s} = \frac{\int_0^t -D\left.\frac{\mathrm{d}C(t)}{\mathrm{d}x}\right|_{x=0}\mathrm{d}t}{s}, \tag{5}$$

where s is the thickness of the TiO_2 film. Eqs. (4) and (5) are interdependent since filling of the sensor will eventually reduce the flux through the interface as the sensor approaches its saturation water concentration c_{sat} when all pores are filled with water. This means that the boundary condition to Eq. (4) at $x = 0$ will depend on c. In this work, $r(t)$ data was used to motivate the choice of boundary conditions as follows. Based on the atmospheric calibration it is a plausible assumption that r will depend linearly on c also in an encapsulated sensor. We can then write $c = -Br + A$, where A and B are unknown positive constants, and write J_0 from Eq. (5) as

$$J_0(t) = s\frac{\mathrm{d}c(t)}{\mathrm{d}t} = -sB\frac{\mathrm{d}r(t)}{\mathrm{d}t}. \tag{6}$$

Furthermore, changes in $c(t)$ can be evaluated with the relation

$$c(t) = c_F + B[r_F - r(t)] \tag{7}$$

where c_F is a constant representing the amount of water which has entered the sensor when the first measurement of r, denoted by r_F, is made. It follows that a plot of $-\mathrm{d}r(t)/\mathrm{d}t$ versus $(r_F - r(t))$ will give a qualitative picture of the dependence of J_0 on c as the sensor is filled with water and approaches saturation. Fig. 8 shows the measured r values in a diffusion experiment for three sensors, S1, S2 and S3, as a function of elapsed time since the pouring of water on top of the EVA. In the beginning of the experiment, sensor resistance was too high to be determined and the first valid measurements conducted just after 2 h gave R values between 10 and 20 MΩ. Fig. 9 shows the $-\mathrm{d}r(t)/\mathrm{d}t$ versus $(r_F - r(t))$ plot calculated from the data in Fig. 8. It is seen that $-\mathrm{d}r/\mathrm{d}t$ remains approximately constant up to about $(r_F - r(t)) = 0.25$, after which all three sensors show an approximately linear decline as they approach the saturation point which corresponds to approximately $(r_F - r(t)) = 0.45$. This information led to the following transport model across the $x = 0$ interface, divided into three separate phases:

(1) An initial phase when the transport across the EVA/TiO_2 interface is limited by the diffusion rate of water through the EVA. This phase was modeled by solving Eq. (4) with boundary conditions $C = 0$ at $x = 0$ and $C = C_{sat}$ at $x = L$, where C_{sat} is the saturation concentration of water in EVA.

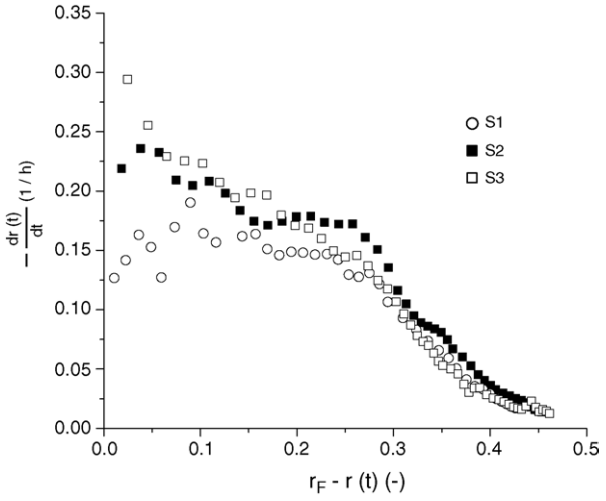

Fig. 9. Plot of $-\mathrm{d}r/\mathrm{d}t$ vs. $(r_F - r(t))$ for the data in Fig. 8. Under the assumption of a linear $r(c)$ function, this corresponds qualitatively to a J_0 vs. c plot.

Table 1
Modeling parameters in encapsulated calibration

General parameters								
D (mm^2/s)			C_{sat} (mg/mm^3)			P (%)		
1.0×10^{-5}			0.005			50		
Sensor-specific parameters								
L (mm)			s (μm)			t_1 and t_2 (h)		
S1	S2	S3	S1	S2	S3	S1	S2	S3
0.551	0.485	0.507	3	3	3	2 and 4	2 and 3.5	2 and 3

General parameters are literature values, sensor-specific parameters were measured. Sensors are labelled S1, S2 and S3.

The latter boundary condition was valid during all three transport phases. Assuming that D is independent of C and that the sensor absorbs water only through its top surface, the water flux J_0 into the sensor in this phase is [14]

$$J_0(t) = -D\left.\frac{dC}{dx}\right|_{x=0} = \frac{DC_{sat}}{L}\left[1 + 2\sum_{n=1}^{\infty}(-1)^n \exp\left(\frac{-Dn^2\pi^2 t}{L^2}\right)\right] \quad (8)$$

(2) An intermediate phase, beginning at $t = t_1$, when the flux remains constant. This phase was modeled by numerically solving Eq. (4) beginning with the water mass concentration distribution at time t_1 and with the boundary condition $J = J_0$ (t_1) at $x = 0$ and $t \geq t_1$.
(3) In the final phase, beginning at time $t = t_2$, the flux decreases linearly as a function of the amount of water in the TiO_2. Eq. (4) was numerically solved beginning with the mass concentration distribution obtained from the previous step at time t_2 and the boundary condition

$$J = J_0(t_1)\left(\frac{c_{sat} - c(t)}{c_{sat} - c(t_2)}\right) \quad \text{at } x = 0 \text{ and } t \geq t_2$$

c_{sat} can be written as $c_{sat} = P\rho$, where P is the porosity of the TiO_2; and ρ, the density of water. The value of $c(t)$ was determined from Eq. (5) throughout the modeling.

The model was solved separately for each sensor using the parameters presented in Table 1. D and C_{sat} for EVA with 33% VA-content were obtained from [15]. The calibration curves showing $r(t)$ as a function of the modeled value of $c(t)$ are shown in Fig. 10. It is seen that the response is approximately linear for all three sensors, but a slight bending is observed when the saturation concentration is approached. This part of the curve is very strongly influenced by the thickness of the TiO_2 film, and the curvature is due to the uncertainty in the thickness measurement which could only be performed to a precision of one significant digit. By modifying the thickness values used in the model slightly, the curves in Fig. 10 can be made linear. In this work, the calibration curve was calculated from the linear parts of the curves in Fig. 10, which give an encapsulated calibration curve

$$r(c) = (1.55 \pm 0.05) - (1.76 \pm 0.06)c\ \text{mm}^3/\text{mg}. \quad (9)$$

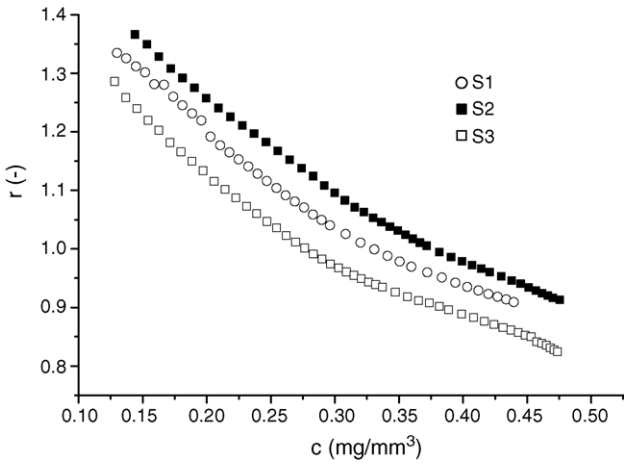

Fig. 10. Encapsulated calibration curves, showing the response as a function of water mass concentration within the sensor for S1, S2 and S3.

The first measurable signals are obtained at a c value of approximately 0.15 mg/mm^3, which corresponds to approximately 10 μg of water within the sensor volume.

4. Discussion

The encapsulated calibration differs from the atmospheric one in two important respects. Firstly, for sensors S1–S3, the lg (R_0) values determined from the atmospheric calibration prior to lamination were equal within a range of 3%, whereas in the data represented in Fig. 8 r values for S1 are consistently 10–20% larger than those of S3 at any given time even when differences in EVA thickness above the sensor is taken into account. This difference may be explained by differences in TiO_2 film thickness, which directly influences the $c(t)$ of an encapsulated sensor through Eq. (5) but does not influence c in an atmospheric measurement since gas adsorption occurs in a uniform manner throughout the porous film. Unfortunately, film thickness could not be measured with sufficient accuracy for studying this question in detail. Secondly, as shown by Eqs. (2) and (9), the sensor has greater sensitivity and lower resistance values in atmospheric than in encapsulated measurements. This is explained by the fact that all the measured water mass concentration will be adsorbed to the TiO_2 film and thus contributing to current transfer in an atmospheric measurement, whereas the penetration of liquid water in a diffusion experiment is likely to leave residual water in the pores which is not carrying current in the sensor.

The transport model used in this work to determine the calibration curve of an encapsulated sensor was developed based on an interpretation of measured resistance data. The linear relationship between r and c in the atmospheric calibration makes this model the most plausible explanation for describing sensor behaviour. It should be emphasized that the model applies to the case where the diffusive flux becomes higher than the

maximum flux across the TiO_2/EVA interface. When the sensor is used in samples mimicking real PV modules, the encapsulant is laminated between two glass sheets and water enters the encapsulant from the vapor phase through the edges of the encapsulant. Since these edges have a very small surface area, the diffusive flux is smaller and the sensor should readily absorb all the water which reaches the TiO_2/EVA interface during the experiment. Sensor placement is of key importance in accelerated aging experiments. The sensitivity of the encapsulated sensor was shown to be on the order of 10 μg, which should be sufficient for making meaningful measurements during accelerated aging experiments. We also note that the high transparency of the entire sensor structure makes it suitable for use on the top glass of a real thin-film PV module without significantly affecting the optical behaviour of the module, which opens up a number of possibilities for new ageing experiments both in the field and in the laboratory.

5. Conclusions

This paper describes a moisture-sensing method for evaluating the protection properties of polymeric encapsulants. It is based on measuring the AC resistance of a porous TiO_2 film covering two interdigitated electrodes on a glass substrate, vacuum laminated under the encapsulation polymer. When open to the environment, the logarithm of the resistance depends linearly on the water concentration in the film, and results indicate that a linear dependence is likely to be valid also in an encapsulated sensor. This sensor has been developed particularly for measurement of moisture concentration in accelerated aging experiments for PV encapsulant polymers such as EVA, but it may also be applicable to other applications in which moisture measurements need to be conducted at the interface between a solid substrate and a polymeric encapsulant.

Acknowledgements

Svenska Litteratursällskapet i Finland rf is gratefully acknowledged for financial support.

References

[1] A.W. Czanderna, F.J. Pern, Encapsulation of PV modules using ethylene vinyl acetate as a pottant: a critical review, Sol. Energy Mater. Sol. Cells 43 (1996) 101–181.
[2] P. Klemchuk, M. Ezrin, G. Lavigne, W. Holley, J. Galica, S. Agro, Investigation of the degradation and stabilization of EVA-based encapsulant in field-aged solar energy modules, Polym. Degrad. Stabil. 55 (1997) 347–365.
[3] N. Allen, M. Edge, M. Rodriguez, C. Liauw, E. Fontan, Aspects of the thermal oxidation, yellowing and stabilization of ethylene vinyl acetate copolymer, Polym. Degrad. Stabil. 71 (2001) 1–14.
[4] N. Dhere, M. Pandit, Study of delamination in acceleration tested PV modules, in: Proceedings of the 17th European PV Solar Energy Conference, Munich, Germany, 22–26 October 2001, pp. 572–575.
[5] T. McMahon, Accelerated testing and failure of thin-film PV modules, Prog. Photov.: Res. Appl. 12 (2004) 235–248.
[6] G. Mon, L. Wen, R. Ross, Water–module interaction studies, in: Conference Record of the 20th IEEE Photovoltaic Specialists Conference, Las Vegas, USA, 26–30 September 1988, pp. 1098–1102.
[7] G. Huyberechts, L. Frisson, In situ formation of humidity-sensitive devices for the evaluation of solar panel encapsulations, Sens. Actuators B 26–27 (1995) 308–311.
[8] E. Traversa, G. Gnappi, A. Montenero, G. Gusmano, Ceramic thin films by sol–gel processing as novel materials for integrated humidity sensors, Sens. Actuators B 31 (1996) 59–70.
[9] Y.-C. Yeh, T.-Y. Tseng, D.-A. Chang, Electrical properties of porous titania ceramic humidity sensors, J. Am. Ceram. Soc. 72 (1989) 1472–1475.
[10] W.-P. Tai, J.-H. Oh, Preparation and humidity sensing behaviors of nanocrystalline bilayered SnO_2/TiO_2 films, Thin Solid Films 422 (2002) 220–224.
[11] G. Garcia-Belmonte, V. Kytin, T. Dittrich, J. Bisquert, Effect of humidity on the ac conductivity of nanoporous TiO_2, J. Appl. Phys. 94 (2003) 5261–5264.
[12] A.L. Myers, Thermodynamics of adsorption in porous materials, AIChE J. 48 (2002) 145–157.
[13] R. Siriwardane, J. Wightman, Interaction of hydrogen chloride and water with oxide surfaces III Titanium dioxide, J. Colloid Interface Sci. 94 (1983) 502–513.
[14] J. Crank, Mathematics of Diffusion, first ed., Oxford University Press, London, 1950, p. 45.
[15] S. Marais, Y. Hirata, D. Langevin, C. Chappey, T. Nguyen, M. Metayer, Permeation and sorption of water and gases through EVA copolymer films, Mater. Res. Innovat. 6 (2002) 79–88.

Biographies

Thomas Carlsson received his MSc degree in engineering physics from Helsinki University of Technology (HUT) in 2001. He is currently a doctoral candidate at the Advanced Energy Systems laboratory, HUT.

Janne Halme received his MSc degree in engineering physics from HUT in 2002. He is currently a doctoral candidate at the Advanced Energy Systems laboratory, HUT.

Peter Lund received his DSc degree in applied physics from HUT in 1984. He is currently professor in Engineering Physics at HUT.

Petri Konttinen received his DSc degree in engineering physics from HUT in 2004. He is currently working as a post-doctoral researcher at the Advanced Energy Systems laboratory, HUT.